JOURNAL OF MAGNETIC RESONANCE **124,** 51–60 (1997)
ARTICLE NO. MN967488

Resonant Modes of the Birdcage Coil

MARK C. LEIFER

Varian Associates, 3120 Hansen Way D-317, Palo Alto, California 94304

Received June 20, 1996; revised September 16, 1996

This paper presents a small and complete set of analytic equations which can be used to design a birdcage coil and predict its resonant modes *a priori* before construction begins. The simple models used include full mutual coupling between all meshes and give the resonant spectrum for both unshielded and shielded coils. The equations are valid, in compact form, for lowpass, highpass, bandpass, and more general birdcage structures. The resonant-mode frequencies are shown to depend on the spatial discrete Fourier transforms of the vectors of electric and magnetic coupling around the coil, making obvious the connection between the resonant and the spatial frequencies of each mode. Inversion of the equations provides values of all of the mesh inductances and couplings from the measured resonance frequencies following coil construction, a result of considerable practical importance. Experimental results are presented which show that these methods regularly predict operating frequencies to a high degree of accuracy for both unshielded and shielded coils.

INTRODUCTION

Since its introduction over a decade ago, the birdcage coil has become a mainstay of NMR imaging and, to some extent, spectroscopy, due to its highly homogeneous transverse RF magnetic field and the ease with which it may be operated in quadrature to produce circularly polarized fields (*1*). Throughout this period, the practical goal of predicting birdcage operating frequencies has remained difficult. On the one hand, empirical approaches are widely used, aided by design guides (*2*) and measurements on portions of coils (*3*), while, on the other hand, there are three-dimensional numerical simulations capable of also accounting for electric fields, loading, and other effects (*4, 5*), but which require sophisticated codes (and users), powerful computers, and sometimes, significant interpretive skills. The approach of this paper lies between these by presenting simple and practical approximate calculations which produce results of useful accuracy, expanding on an earlier such treatment (*6*). Quasistatic models possessing analytic solutions are used throughout, because the formulas they produce are generally easily understood and readily evaluated. Experiments with coils of dimensions up to one-eighth of a free-space wavelength show that the model calculations can usefully predict birdcage performance, can aid in choosing dimensions and capacitor values before construction begins, and can minimize or eliminate the iterative tuning/rebuilding which has often accompanied practical birdcage construction.

To this end, a solution for the resonant modes of the birdcage using the mesh eigenvalue approach of Tropp (*7*) and Joseph and Lu (*8*) is presented which makes clear the dual transform nature of the solution. Although portions of this treatment have appeared elsewhere, the presentation here is rigorous, and the results are of wider scope than previous treatments and motivate new results. The inversion procedure of the second section is one such new result and shows how all the inductance values can be derived from the resonant frequencies measured for a birdcage coil. This result is used to check the accuracy of the inductance calculations presented in the third section, which, for the practical-minded reader interested in predicting coil behavior, contains perhaps the most important new information. There, analytic equations for carefully chosen approximate models are presented and used to describe the coil. The last section shows that the predictions agree closely with observations from actual coils, in some cases to within a fraction of a percent. A preliminary report of this work as applied to lowpass coils has appeared separately (*9*).

RESONANT AND SPATIAL MODES OF THE COUPLED BIRDCAGE

Consider a symmetric N-leg ''bandpass'' birdcage containing capacitors in both its endrings and legs, a portion of which is shown in Fig. 1. This structure includes the lowpass and highpass coils as special cases when $1/C1$ or $1/C2$ is set to zero. We label the inductance of a single mesh L_{mesh}, note that the flux coupling M_m between any two meshes depends only on their separation m, and define $M_0 = L_{\text{mesh}}$ for convenience. Where earlier treatments sum self- and mutual inductances into single terms (*7*) or neglect some inductance contributions (*8*), an effort has been made here to present a consistent and complete treatment. Kirchoff's mesh equations transformed to the complex s plane give the system of coupled equations

1090-7807/97 $25.00

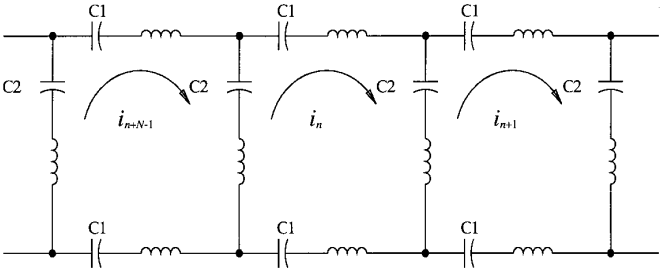

FIG. 1. A section of the birdcage transmission line showing mesh currents I_n. The line is periodic, that is, the left- and right-most ends are connected together.

$$s^2 \sum_{m=0}^{N-1} I_{n+m} M_m + 2I_n \left(\frac{1}{C1} + \frac{1}{C2} \right) - \frac{1}{C2} (I_{n+1} + I_{n+N-1}) = 0, \quad [1]$$

where n (and below, the indices k and m) take the integer values zero to $N - 1$ unless otherwise noted, and where all indices are modulo N so that, for example, $I_{n+N} = I_n$. There is an additional mode arising from equal currents flowing in the same direction in each end ring, which cannot be constructed of any combination of currents shown in Fig. 1. The mesh equations may be dispensed with in this case and the resonance frequency for this mode, called the co-rotating (CR) ring mode, written immediately as

$$\omega_{\mathrm{CR}} = \sqrt{\frac{N}{C1(L_{\mathrm{ring}} + M_{\mathrm{ring}})}}, \quad [2]$$

where L_{ring} is the self-inductance of each ring and M_{ring} is the mutual inductance between them. This mode differs from the others in that it has no waves propagating around the coil meshes and does not produce a transverse magnetic field in the sample region. The position of this mode in the resonance spectrum will be discussed below.

To find the other modes, Eq. [1] is put into the form of a generalized eigenvalue problem

$$\mathbf{E}\mathrm{I} = \lambda \mathbf{M}\mathrm{I}, \quad [3]$$

where $\lambda = s^2$, and the matrices $\mathbf{E}$ and $\mathbf{M}$ contain the electric and magnetic coupling terms, respectively. Because these matrices are *circulant*, reflecting the periodic nature of the birdcage structure, solutions have the form of discrete Fourier transforms (DFTs). The formal solution to the eigenvalue problem is presented in the Appendix to make the point that the eigenvalues $\lambda_k = -\omega_k^2$ of the birdcage coil are given by the beautifully simple equation

$$\lambda_k = \frac{\tilde{E}_k}{\tilde{M}_k}, \quad [4]$$

where $\tilde{E}_k$ and $\tilde{M}_k$ are the eigenvalues of the mutual inductance and mutual capacitance matrices, or, equivalently, the spatial transforms of the electric and magnetic couplings in the coil. This formulation of the eigenvalue solution has two advantages: first, Eq. [4] is general and applies to other symmetric and periodic mesh structures [the dome (*11*) and free-element (*12*) resonators are two examples] by placing appropriate entries in $\mathbf{E}$ and $\mathbf{M}$, and second, it may be inverted to solve for either electric or magnetic coupling, as shown in the next section.

For the birdcage structures under consideration here, the spatial transform quantities evaluate to

$$\tilde{M}_k = \sum_{m=0}^{N-1} M_m \exp(-i2\pi km/N) \quad [5]$$

and

$$\tilde{E}_k = -2\left[\frac{1}{C1} + \frac{1}{C2} \left(1 - \cos \frac{2\pi k}{N} \right) \right], \quad [6]$$

as shown in the Appendix, giving a practical form for the resonant frequencies of the birdcage coil

$$\omega_k = \sqrt{\frac{2}{\tilde{M}_k} \left[\frac{1}{C1} + \frac{1}{C2} \left(1 - \cos \frac{2\pi k}{N} \right) \right]}. \quad [7]$$

As is well known, the symmetry of $\mathbf{E}$ and $\mathbf{M}$ ($M_m = M_{N-m}$) results in the $N/2 - 1$ degenerate eigenvalue pairs which permit practical quadrature operation (*7*). The resonant frequencies are those at which a propagating wave has an integral number k of wavelengths around the structure, so k is the index of spatial frequency in cycles per revolution, also known as the wavenumber (*13*). The expression in Eq. [7] is therefore the discrete ω vs k dispersion relation for waves traveling around the birdcage transmission line. It has been appreciated since the birdcage's invention that higher-order modes correspond to patterns of higher spatial frequency (*1*), but it is worth noting that the correspondence is contained explicitly in the formulas for the resonant frequencies.

Where does the CR ring mode of Eq. [2] fit into the resonance spectrum? Its close relative is the $k = 0$ mode, which has equal and opposite ring currents and zero leg currents, is also called the anti-rotational (AR) ring mode in this paper, and has resonant frequency

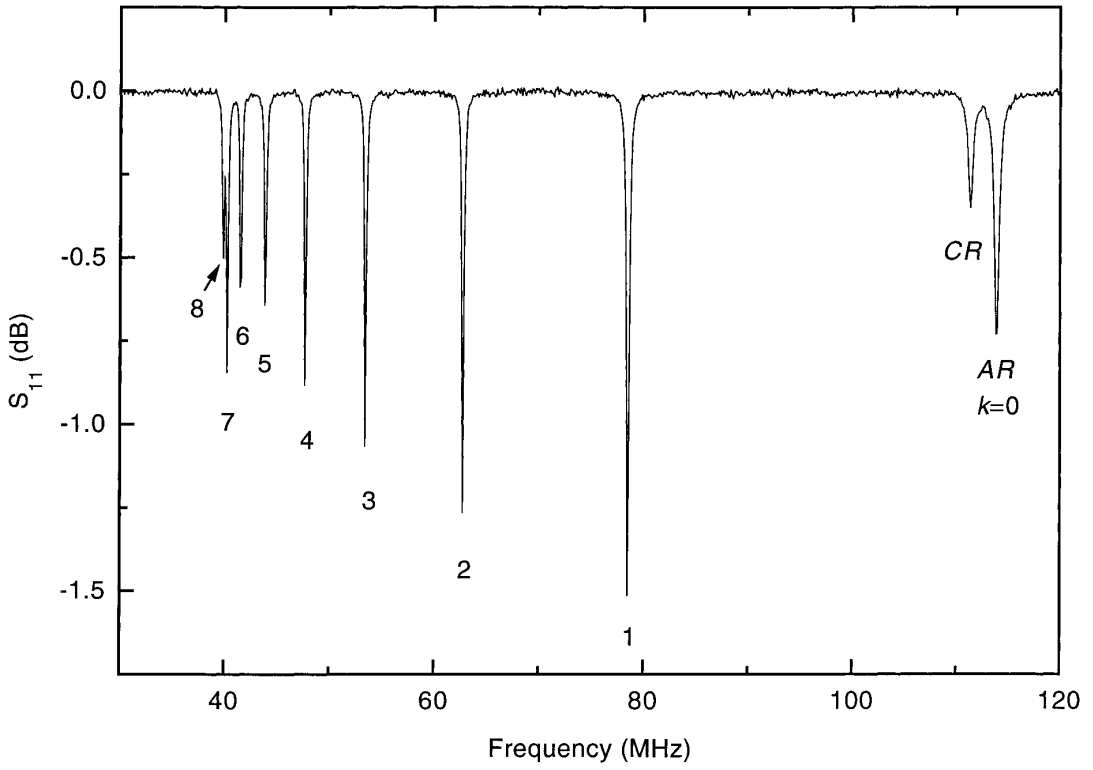

FIG. 2. The resonance spectrum measured from a 16-leg highpass coil. The modes are labeled, with AR and CR being the anti- and co-rotational modes described in the text.

$$\omega_{\mathrm{AR}} = \omega_0 = \sqrt{\frac{N}{C1(L_{\mathrm{ring}} - M_{\mathrm{ring}})}} \qquad [8]$$

by analogy to Eq. [2]. The modes ω_{CR} and ω_{AR} form a doublet with ω_{CR} lower in frequency, except in the lowpass coil where they are degenerate at zero frequency. Figure 2 shows the resonance spectrum of an $N = 16$ highpass coil labeled to identify the AR/CR ring mode doublet, seven degenerate mode pairs labeled by their lowest mode number $k = 1 \ldots 7$, and $k = 8$ singlet mode. In a lowpass spectrum, the ring mode doublet becomes degenerate at zero frequency, with higher-order modes increasing in frequency.

Earlier work on birdcage resonant frequencies includes an extensive treatment of the highpass coil in which spatial properties are discussed and in which the DFT is mentioned but in which the end-ring inductances are neglected (*8*), and a brief treatment of the coupled lowpass (*14*) which, however, reports a formula different from that derived here. Several approximations considering only nearest-neighbor couplings have appeared (*7, 15, 16*), the latter including an examination of the (approximate) dispersion relations. Finally, a recent abstract treating the dome resonator presents a form of the correct resonance formula, but with little elaboration (*11*).

INVERTING THE MODE EQUATIONS

The existence of dual transforms in Eq. [4] means that, if the birdcage resonance frequencies are known, then either **M** or **E** may be found in terms of the other through application of the inverse discrete Fourier transform. In most cases, the capacitance values are known but the inductance values are not, so we invert Eq. [5] to give the coupling values in terms of the measured resonance spectrum ω_k,

$$M_m = \frac{1}{N} \sum_{k=0}^{N-1} \tilde{M}_k \exp(i2\pi km/N) \,, \qquad [9]$$

where $\tilde{M}_k$ is given for the bandpass coil by

$$\tilde{M}_k = \frac{2}{\omega_k^2} \left[\frac{1}{C1} + \frac{1}{C2} \left(1 - \cos \frac{2\pi k}{N} \right) \right] . \qquad [10]$$

This is a new result with considerable practical importance—since frequency can be measured precisely, we can now find the mesh self- and mutual inductances to an accuracy given by the capacitor tolerance.

In the next section, this inversion will be used to check the accuracy of birdcage inductance calculations, but first we discuss some calculational details. Note that each M term is a sum over all measured mode frequencies, so that random measurement errors tend to average away and an error in any one value is spread out, making this a numerically robust inversion. For bandpass and highpass coils, Eqs. [9] and [10] are evaluated just as written (either by explicit summation or with an FFT algorithm) and we may proceed to the next section. The lowpass coil presents the problem of an indeterminate $k = 0$ term in the summation, however, because $1/C1$, $[1 - \cos(0)]$, and ω_0 are all zero. To understand the physical reason for this, remember that direct current flows in the end-rings in this mode; these currents, and the overall mode inductance, are unaffected by any potential between the rings and, therefore, by any DC energy stored in the leg capacitors, so the mode has indeterminate electrical energy. The total mode inductance $N\tilde{M}_0$ is still finite and well behaved even though it cannot be measured directly in the lowpass coil, so we expect to be able to estimate it accurately since the frequency measurements are relatively precise. We make use of knowledge about the system in choosing an appropriate technique.

The most general model of this finite-length discrete linear system is the ARMA (autoregressive-moving average) model in the complex z plane consisting of a rational polynomial function in z (*10*), where the order (number of poles and zeroes) must not exceed the order of the system N. Because of the difficulty of estimating the parameters of an ARMA model, it is common practice to use an all-pole (autoregressive or AR) model instead (*10, 17*), and the present system is consistent with an all-pole model: the transform (''spectrum'') given by Eq. [9] has no zeroes on the unit circle, and it must have poles since $\tilde{M}_k$ is periodic for k ranging from minus to plus infinity. We therefore use linear prediction, a robust AR estimator which generally gives good results for smooth oscillatory sequences, to estimate $\tilde{M}_0$ from the $N - 1$ other measured $\tilde{M}$ values; following this, the inductance values M_m may be calculated from Eq. [9] as they are for the band- and highpass coils.

It remains to choose the estimator model order P. Linear prediction algorithms are known to perform best with few free parameters, the measured $\tilde{M}_k$ sequence has only $N/2$ independent values, and we are predicting only the next point in the sequence, so it makes sense to choose P less than $N/2$. To verify this, a linear prediction algorithm (*18*) was used to estimate $\tilde{M}_{16}$ (which is identical to $\tilde{M}_0$) from $\tilde{M}_1 \ldots \tilde{M}_{15}$ measured for the 16-leg highpass coil whose spectrum appears in Fig. 2 and which is described later. $\tilde{M}_0$ was also measured directly for comparison. The linear prediction estimate is within 1.5% of the measured value of 21.7 nH for P between 3 and 8, with larger deviations for P outside this range. Keep in mind that $\tilde{M}_0$ is summed with $N - 1$ much larger values in Eq. [9], so its estimation error degrades the accuracy of the derived inductance values in only a small way, as noted earlier. These considerations support the use of a linear predictor with, say, $P = 6$ for the 16-leg lowpass coil in the final section below where $\tilde{M}_0$ is not known.

As a point of interest, we mention a direct but ill-advised method of determining $\tilde{M}_0$. Note that only M_0 survives the sum on the right side of Eq. [5] for $k = N/2$, allowing us to determine $M_0^{(\mathrm{est})}$ from the measured value $\omega_{N/2}$ through Eq. [10]. A rearrangement of Eq. [9] then gives the direct formula

$$\tilde{M}_0 = NM_0^{(est)} - \sum_{k=1}^{N-1} \tilde{M}_k = N\tilde{M}_{N/2} - \sum_{k=1}^{N-1} \tilde{M}_k, \quad [11]$$

where all terms on the right are derived from measurements. This method commits three numerical analysis sins, however; it derives $M_0^{(\mathrm{est})}$ from a single measured datum, then multiplies it by N which increases by a large factor any error in its value, and finally, forms the answer as the small difference between this big number and another big number. Even carefully collected data are unlikely to produce an accurate estimate this way. By contrast, the linear prediction technique finds $\tilde{M}_0$ as the next in a sequence of similar-sized values by using a smoothing process, producing a far better estimate.

To summarize this section, analysis of the birdcage mesh structure in terms of transforms permits us to find the M_m values from the measured resonance frequencies by inverse transform, immediately in the case of bandpass and highpass coils. For the lowpass coil, the term $\tilde{M}_0$ is ''hidden'' because there is no current flowing through the leg capacitors in the $k = 0$ mode and, hence, no resonance with which to read out the value. This value is recovered with linear prediction, a technique suited to the smooth periodic nature of the data sequence. The estimated value is then used in the inversion formula to find the lowpass inductance values.

CALCULATING BIRDCAGE INDUCTANCES

Birdcage calculations can proceed at various levels of sophistication, with the most accurate results coming from numerical solutions of Maxwell's equations, typically using finite-element or difference algorithms. It is the aim of the remaining sections to show that fairly simple models can also give excellent results and offer the advantage of having analytic expressions which make computation a relatively straightforward matter. A related transmission-line approach specific to eight-leg coils has appeared (*6*), but it will be seen that the following calculations are more general, apply to coils with RF shields, and give more accurate results.

Foil conductors on a cylindrical form of radius r_0 are used throughout.

The inductance term M_m is the sum of mutual couplings between every nonorthogonal pair of conductors in the two meshes m apart,

$$M_m = 2Mleg_m - Mleg_{m-1} - Mleg_{m+1} + 2(Mrs_m - Mrs'_m). \quad [12]$$

The simplest way to calculate the individual terms is to use static handbook formulas for the contributions of each conductor. Here $Mleg_m$ is the mutual inductance between legs calculated by the appropriate formula below (with $Mleg_0$ being the self-inductance of a single leg), Mrs_m [Mrs'_m] is the mutual inductance between ring segments in the same [opposite] ring[s], and the signs are derived from the senses of the mesh currents in Fig. 1.

For all but leg couplings in a single and between nearest-neighbor meshes, comparison to values derived with Eq. [9] from coil observations shows that it is sufficient to replace the leg and ring strips by equivalent filaments at their centers. This approximation is partially motivated by the relative insensitivity of inductance to details of the distribution of the current supporting it—the field energy in the volume outside of the conductor contributes most to the inductance, and only the small contributions from regions close to the conductor are affected by the actual current distribution within—and is backed by solid experimental confirmation. The handbook formula giving the mutual inductance in henries between two legs (or more specifically, two parallel filaments) of length h and separation s in meters is

$$Mfil(s) = \frac{\mu_0 h}{2\pi}\left[\ln\left(\frac{h}{s}+\sqrt{1+\left(\frac{h}{s}\right)^2}\right)-\sqrt{1+\left(\frac{s}{h}\right)^2}+\frac{s}{h}\right]. \quad [13]$$

This and other formulas and methods discussed in this section are found in (*19*). For coupling between noncontiguous ring segments, Neumann's formula gives

$$Mrr = \frac{\mu_0 r_0 r_1}{4\pi}\int_0^{\theta}\int_{\theta'}^{\theta'+\theta} \times \frac{\cos(\theta_2-\theta_1)}{\sqrt{r_0^2+r_1^2-2r_0r_1\cos(\theta_2-\theta_1)+s^2}}\,d\theta_2 d\theta_1, \quad [14]$$

where the ring segments are w wide, θ long, and separated by (s, θ'), and where $r_1 = r_0$ for the unshielded birdcage (the different radii accomodate later shield calculations). The mutual inductance between adjacent ring segments is approximated by that of two joined straight filaments of length $h = 2r_0\sin(\pi/N)$ inclined at an angle $\phi = \pi - 2\pi/N$,

$$Mincl = -\frac{\mu_0 h\cos\phi}{\pi}\tanh^{-1}\left[\frac{1}{1+\sqrt{2(1-\cos\phi)}}\right]. \quad [15]$$

For better accuracy in the dominant single mesh and nearest-neighbor inductance terms, consider the strips to be a collection of infinitely many parallel filaments, all of which contribute equally. This uniform current distribution throughout the conductor is a compromise between the simplistic single-filament approximation and the true high-frequency distribution, and has the advantage of being mathematically tractable. The self-inductance of a ring or leg in a single mesh is then approximated by that of a flat thin strip

$$Lstrip = \frac{\mu_0 h}{2\pi}\left(\ln\frac{2h}{w}+\frac{1}{2}\right), \quad [16]$$

where w is the width and h the length. For the mutual inductance of two legs $2\pi n/N$ apart in either single or adjacent meshes on a cylinder, integration of Eq. [13] over their width $\delta\theta$ gives

$$Mcyl = \delta\theta^{-2}\int_0^{\delta\theta}\int_{(2\pi n/N)}^{(2\pi n/N)+\delta\theta} \times Mfil\left(2r_0\sin\frac{\theta_2-\theta_1}{2}\right)d\theta_2 d\theta_1, \quad [17]$$

which includes curvature of the leg foil over its width. The argument of *Mfil* gives the distance between the filaments being integrated. Finally, the mutual inductance between the (approximately) flat leg or ring strips of width w and their parallel images will be needed for shield calculations,

$$Mpar = w^{-2}\int_0^{w}\int_{s}^{s+w} \times Mfil(\sqrt{(x_2-x_1)^2+(r_1-r_0)^2})\,dx_2 dx_1. \quad [18]$$

The preceeding double integrals give the same results as would the comparable Neumann's formulas having quadruple integrals, but evaluate in a fraction of the time.

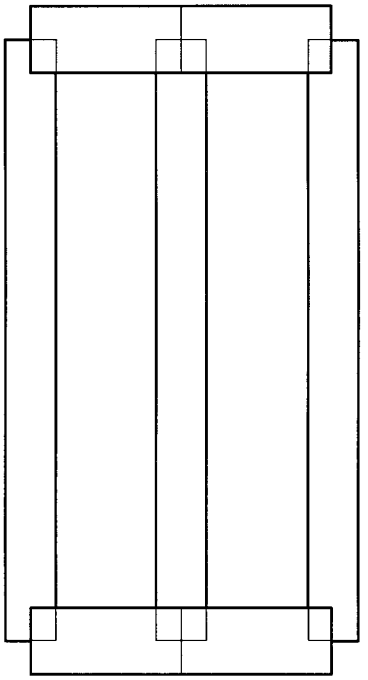

FIG. 3. A two-mesh segment of the birdcage foil conductors, showing how the strips are sized for the handbook-formula inductance calculations.

Note that Eqs. [5], [7], and [8] give an equation for the total inductance $N\tilde{M}_0$ of the $k = 0$ mode,

$$N \sum_{m=0}^{N-1} M_m = 2(L_{\text{ring}} - M_{\text{ring}}). \qquad [19]$$

This identity, which can also be verified (albeit tediously) by explicit summation of Eq. [12], gives a convenient overall accuracy check on the computations of M_m since exact analytic expressions are available for the right-hand side (*20*). A good match here lends confidence to the final frequency predictions, making this a valuable gage for the computational design technique.

COMPARISON TO MEASUREMENTS

To illustrate the principles outlined so far, consider a 16-leg birdcage 8.9 cm diameter by 12.8 cm long with 1 cm wide end-rings and 0.635 cm wide legs. Figure 3 shows how the strips were sized for the handbook formula calculations of Eqs. [13]–[17], which give $M_0 = 122$ nH and other values as shown in the first column of Table 1 (only the first $N/2 + 1$ values are listed since $M_{N-m} = M_m$). The values of M_m calculated by these methods give a checksum in Eq. [19] of 334 nH which is within 1.5% of the independently calculated value of 338 nH, a good indication that the frequency predictions will be accurate, as well.

TABLE 1
Calculated and Measured Inductance of Unshielded Coils

n	M_n (model) (nH)	M_n (lpmeas) (nH)	M_n (hpmeas) (nH)
0	122	117	115
1	−38.1	−36.4	−34.9
2	−6.1	−5.3	−5.3
3	−2.3	−2.3	−2.3
4	−1.4	−1.4	−1.3
5	−1.0	−0.9	−0.8
6	−0.8	−0.9	−0.8
7	−0.8	−0.7	−0.8
8	−0.7	−0.8	−0.8

For comparison purposes, two birdcages of this size were constructed of etched copper foil. A 300 pF 5% tolerance microwave chip capacitor was placed at every leg/ring junction (C2 = 150 pF) of the first coil to form a lowpass structure, while C1 = 180 pF 2% chips in the endrings of the second formed a highpass coil. The resonances were measured with a network analyzer and a loosely coupled loop and are listed in Table 2. Inductance terms for the highpass coil were evaluated directly from Eqs. [8] [the measured value of $2(L_{\text{ring}} - M_{\text{ring}})$ is 347 nH, close to the independently calculated checksum value], [9], and [10]. For the lowpass coil, the linear prediction method of the previous section with $P = 6$ was applied to the 15 measured values of Eq. [10] to give $\tilde{M}_0 = 20.1$ nH, which was then used in Eq. [9] with the measured values. All of the transform data for low- and highpass coils are plotted in Fig. 4 (the largest descrepancy between them is 2.3% at $k = 8$ which is well within

TABLE 2
Calculated and Measured Resonant Frequencies of Unshielded Coils

n	f_n^{lp} (model) (MHz)	f_n^{lp} (meas.) (MHz)	f_n^{hp} (model) (MHz)	f_n^{hp} (meas.) (MHz)
0	0	0	116	114
CR	0	0	113	112
1	23.7	24.1	78.3	79.1
2	36.5	37.4	61.5	63.2
3	44.7	45.9	51.9	53.5
4	50.5	51.9	46.1	47.7
5	54.6	56.1	42.4	44.0
6	57.5	58.8	40.2	41.6
7	59.2	60.4	39.0	40.3
8	59.7	61.0	38.6	39.9

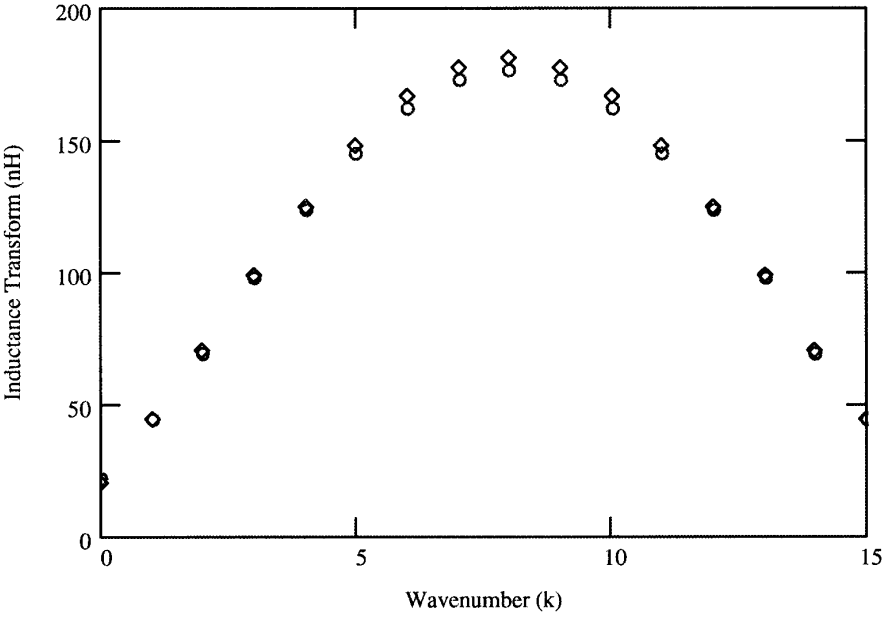

FIG. 4. Plot of the mutual inductance transform vector $\tilde{\mathbf{M}}$ as a function of mode or wavenumber. Values are measured from 16-leg highpass (circles) and lowpass (diamonds) coils, with the lowpass $\tilde{M}_0$ value estimated by linear prediction as described in the text.

the combined capacitor tolerance), and the M values derived from them are listed in Table 1.

The observed M_0 values of 117 and 115 nH for this coil match the calculated handbook value of 122 nH to 4–6%, the deviation being somewhat larger than that expected from the capacitor tolerance. It is clear from the table that the nearest-neighbor value (which has opposite sign) is also overestimated by the handbook formulas, and by enough that the errors largely cancel in the summations for the resonance frequencies. Indeed, experience shows that this overestimation and error cancellation is stable for coils of many sizes and aspect ratios, leading to consistently excellent frequency estimates as shown below.

The lowpass calculated (diamond) and measured (cir-

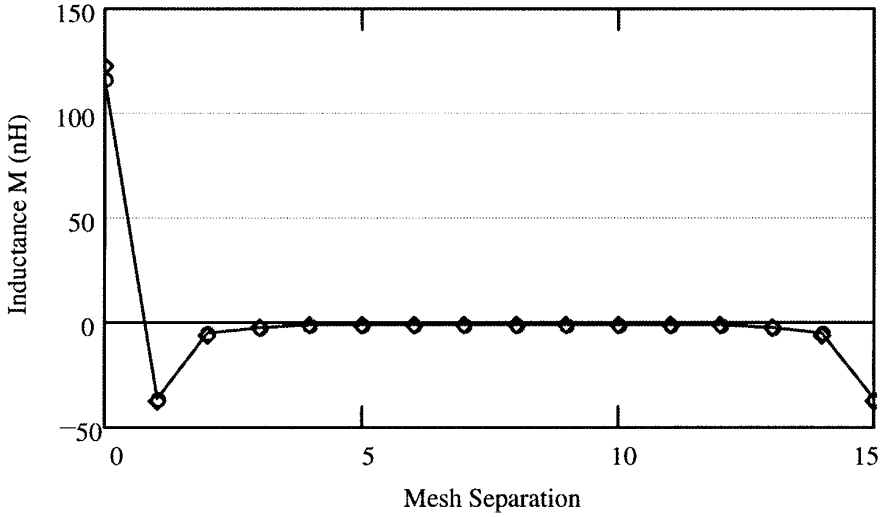

FIG. 5. A plot of the self- (M_0) and mutual-inductance values for the lowpass coil as a function of mesh separation. Diamonds give calculated values, while circles and solid line show measured values. This sequence and that of Fig. 4 form a discrete Fourier transform pair.

cles and solid line) values of the M vector plotted in Fig. 5 show the expected symmetry and close agreement of observed and computed values. The coupling quickly becomes small beyond the nearest-neighbors, leading to the common practice of including only nearest-neighbor coupling in approximate calculations. Still, improved accuracy results from inclusion of all terms, as has been noted earlier (*14, 16*).

Finally, the self- and mutual-inductance values calculated from the coil geometry and listed in Table 1 are used with Eqs. [5]–[7] to predict the birdcage resonant frequencies, which are given in Table 2 together with spectra measured from the actual coils. The frequency of the CR mode calculated from Eq. [2] is also presented. The predicted frequencies for the $k = 1$ homogeneous-field mode most useful for NMR are within 1.7 and 1.0% of the observed lowpass and highpass values. Experience with numerous other coils shows accuracy to consistently be within about one-half of the capacitor tolerance. Obviously, this is a useful aid for choosing capacitor values to resonate a given coil geometry to a desired frequency, or in choosing coil dimensions to resonate there with available capacitors.

SHIELDED COILS

A practical discussion of birdcage coils is not complete without mentioning the effects of an RF foil shield surrounding the coil. Such shields increase resonance frequencies and decrease both field strength and homogeneity, but are widely used to reduce interactions between coil and environment. Their analysis lies at the limits of validity of simple models with analytic solutions, however. The common suggestion of accounting for shield effects by including mutual coupling to image currents is problematic, since simple images assume conducting sheets of infinite extent. In an early such study, inductances for a doubly resonant highpass coil calculated with Neumann's formula for both legs and leg images (rings were neglected) gave resonant frequencies which matched observations only to within about 15% (*8*). Image locations were found by considering infinite line currents flowing parallel to an infinitely long cylindrical conducting shield, which is a poor approximation for finite legs whose length is approximately equal to the shield diameter, and is certainly wrong for short ring segments transverse to the cylinder axis. Furthermore, experimental evidence shows that other effects are also important. For instance, electric coupling between parts of the birdcage to the shield is ignored in the simple models presented here, and the CR mode of the 16-leg highpass coil considered above is so severely disturbed by the presence of a shield 13.3 cm in diameter and 18.7 cm long that its resonance in Fig. 2 completely disappears.

Despite these conceptual uncertainties, a calculation including mutual coupling to image currents was applied to the coils of this paper. A shield of radius r_s is approximated in the vicinity of each conductor as an infinite conductive plane, a more reasonable assumption than that of a cylinder for reasons just mentioned, giving an image located an equal distance behind the plane at a radius $r_1 = 2r_s - r_o$. Ring segments are assumed to have images of the same angular extent. Values of $\mathbf{M}$ and $\tilde{\mathbf{M}}$ in expressions throughout this paper now become effective values which have been reduced by coupling to the image currents. Calculations follow the unshielded ones outlined in the previous section, with each term in Eq. [12] modified by a correction representing the mutual inductance between the corresponding image currents. Specifically, self-inductance of the single-mesh elements is reduced by mutual coupling of a leg or ring segment to its own image, calculated with Eq. [18] as that between parallel flat strips. Mutual inductances between leg images are computed as between parallel filaments using Eq. [13], and between ring images using Eq. [14], except for the images of contiguous ring segments which are calculated at r_1 with Eq. [15]. These calculations applied to the 13.3 cm diameter shield surrounding the low- and highpass coils correctly predict the $k = 1$ observed frequencies of 27.7 and 89.9 MHz to within 1.4 and 0.7%, respectively. The M_0 and M_1 terms are still overestimated compared to highpass measurements obtained with Eq. [9], so the accuracy of the frequency estimate is aided, again, by offsetting errors. As was found for the bare coils, this error cancellation is consistent for the shielded coils and does not diminish the usefulness of the technique.

To further show the practical value of the model calculations, and to demonstrate that they retain their validity at high frequencies, predicted $k = 1$ mode frequencies were compared to observed values for a variety of shielded birdcage coils operating at 200 MHz. The frequency predicted for an 8.9/13.3 cm (winding/shield diameter) 8-leg lowpass coil agreed with experiment to within 1.6%, those for 7/12.1 and 11.4/15.2 cm 16-leg lowpass coils were both within 1.3% and, finally, those for 16.5/21 cm 8-leg lowpass and bandpass coils with precision capacitors were predicted to 0.4 and 0.6%. Despite the theoretical uncertainty behind this simple treatment of the shield, it gives consistently good results for a variety of sizes and styles at both low and high frequencies.

In conclusion, this paper has shown how simple models can describe birdcage coil behavior with analytic equations which are straightforward to understand and evaluate. The formula for the frequencies of the resonant modes explicitly shows the link to the spatial frequencies of electric and magnetic coupling in the coil, with applicability to other periodic mesh structures, and its inverse allows

the inductance coupling values to be found from measured frequencies. Of perhaps greatest practical value are the simple methods and equations which predict resonant frequencies from the chosen geometry and dimensions without the need to construct or test any mockups; these are shown to agree to a high degree of accuracy with measurements on both bare and shielded coils at usefully high frequencies.

APPENDIX

The formal solution to the birdcage mesh problem is outlined briefly below to show that the eigenvalues and coupling terms are expressed naturally in terms of the DFT. The mesh equations are written as the generalized eigenvalue problem of Eq. [3] with

$$\mathbf{M} = \begin{bmatrix} M_0 & M_1 & \cdot & \cdot & M_{N-1} \\ M_{N-1} & M_0 & \cdot & \cdot & M_{N-2} \\ \cdot & & \cdot & & \cdot \\ \cdot & & & \cdot & \cdot \\ M_1 & M_2 & \cdot & \cdot & M_0 \end{bmatrix}, \mathbf{I} = \begin{bmatrix} I_0 \\ I_1 \\ \cdot \\ \cdot \\ \cdot \\ I_{N-1} \end{bmatrix}, \quad [A1]$$

and

$$\mathbf{E} = \begin{bmatrix} -2\left(\frac{1}{C1}+\frac{1}{C2}\right) & \frac{1}{C2} & 0 & \cdot & \frac{1}{C2} \\ \frac{1}{C2} & -2\left(\frac{1}{C1}+\frac{1}{C2}\right) & \frac{1}{C2} & \cdot & 0 \\ \cdot & & \cdot & & \cdot \\ \frac{1}{C2} & 0 & \cdot & \frac{1}{C2} & -2\left(\frac{1}{C1}+\frac{1}{C2}\right) \end{bmatrix}. \quad [A2]$$

As pointed out in the text, the matrices $\mathbf{M}$ and $\mathbf{E}$ are circulant and therefore possess special eigenvalue properties. The kth eigenvector of any circulant matrix $\mathbf{M}$ is equal (within a constant) to the kth vector $\mathbf{W}^k$ of complex coefficients of the N-point DFT (*10*), the mth row or element of which is

$$W^k_m = \exp(-i2\pi km/N). \quad [A3]$$

The $\mathbf{W}^k$ are also the mesh currents or eigenvector solutions to the birdcage problem (to within a constant i_0) because Eq. [3] can be rewritten as a standard eigenvalue problem $\mathbf{AI} = \lambda\mathbf{I}$ whose matrix $\mathbf{A} = (\mathbf{M}^{-1}\mathbf{E})$ is still circulant (*21*). Since all circulant matrices have the same eigenvectors $\mathbf{W}^k$, $\mathbf{I}^k = i_0\mathbf{W}^k$ follows directly.

The vector $\tilde{\mathbf{M}}$ of eigenvalues $\tilde{M}_k$ of the circulant matrix $\mathbf{M}$ is given by the DFT expression

$$\tilde{\mathbf{M}} = (\mathbf{W}^k)^{\mathrm{T}}\mathbf{M}, \quad [A4]$$

where T denotes transpose and $\mathbf{M}$ is the column vector of elements M_m (*10*). Since any matrix may be expanded in a similarity transformation in terms of its eigenvalues and -vectors, $\mathbf{M}$ in Eq. [3] can be factored as

$$\mathbf{M} = \mathbf{I}\boldsymbol{\mu}\mathbf{I}^{\mathrm{H}}, \quad [A5]$$

where the columns of $\mathbf{I}$ are the eigenvectors $\boldsymbol{I}^k$, H denotes the hermitian conjugate, and $\boldsymbol{\mu}$ is a diagonal matrix of the eigenvalues $\tilde{M}_k$. If $\mathbf{E}$ is similarly factored in terms of the diagonal matrix of its eigenvalues $\tilde{E}_k$, then the system eigenvalues λ_k of Eq. [3] reduce with standard matrix manipulations to the ratio of matrix eigenvalues $\tilde{E}_k/\tilde{M}_k$. This is the formal solution to the problem and is completely general for any structure having matrices $\mathbf{E}$ and $\mathbf{M}$ which are circulant.

A specific expression for the bandpass coil (containing the low- and highpass coils as special cases) is readily found. $\tilde{M}_k$ is expanded as Eq. [5] and the transform for $\tilde{E}_k$ with the values of Eq. [A2] reduces to Eq. [6] for integer k, giving the final expression in Eq. [7].

REFERENCES

1. C. Hayes, W. Edelstein, J. Schenck, O. Mueller, and M. Eash, *J. Magn. Reson.* **63,** 622–628 (1985).
2. T. Vullo, R. Zipagan, R. Pascone, J. Whalen, and P. Cahill, *Magn. Reson. Med.* **24,** 243–252 (1992).

3. J. Tropp, Abstracts of the Society of Magnetic Resonance in Medicine, 11th Annual Meeting, p. 273, 1992.
4. H. Ochi, E. Yamamoto, K. Sawaya, and S. Adachi, Abstracts of the Society of Magnetic Resonance in Medicine, 12th Annual Meeting, p. 1356, 1993.
5. Q. Yang, H. Maramis, S. Li, and M. Smith, Abstracts of the Society of Magnetic Resonance, 2nd Annual Meeting, p. 1110, 1994.
6. R. Pascone, T. Vullo, J. Farrelly, and P. Cahill, *Magn. Reson. Imaging* **10,** 401–410 (1992).
7. J. Tropp, *J. Magn. Reson.* **82,** 51–62 (1989).
8. P. Joseph and D. Lu, *IEEE Trans. Med. Imaging* **8,** 286–294 (1989).
9. M. Leifer, Abstracts of the International Society of Magnetic Resonance in Medicine, 4th Annual Meeting, p. 1420, 1996.
10. S. Marple, ''Digital Spectral Analysis,'' Chaps. 3, 6–8, Prentice-Hall, Englewood Cliffs, New Jersey, 1987.
11. R. Srinivasan and H. Liu, Abstracts of the International Society of Magnetic Resonance in Medicine, 4th Annual Meeting, p. 1425, 1996.
12. H. Wen, A. Chesnick, and R. Balaban, *Magn. Reson. Med.* **32,** 492–498 (1994).
13. L. Brillouin, ''Wave Propagation in Periodic Structures,'' 2nd ed., Dover, New York, 1953.
14. J. Tropp, Abstracts of the Society of Magnetic Resonance in Medicine, 12th Annual Meeting, p. 1347, 1993.
15. J. Tropp, Abstracts of the Society of Magnetic Resonance in Medicine, 11th Annual Meeting, p. 4009, 1992.
16. R. Pascone, B. Garcia, T. Fitzgerald, T. Vullo, R. Zipagan, and P. Cahill, *Magn. Reson. Imaging* **9,** 395–408 (1991).
17. T. Ulrych and M. Ooe, *in* ''Nonlinear Methods of Spectral Analysis'' (S. Haykin, Ed.), 2nd ed., Chap. 3, p. 73–125, Springer-Verlag, Berlin, 1983.
18. W. Press, B. Flannery, S. Teukolsky, and W. Vetterling, ''Numerical Recipes in C,'' Chap. 12, Cambridge Univ. Press, Cambridge, 1988.
19. F. Grover, ''Inductance Calculations: Working Formulas and Tables,'' Dover, New York, 1962.
20. C. Snow, ''Formulas for Computing Capacitance and Inductance,'' NBS Circular 544, Sects. 2.4 and 2.7, U.S. Government Printing Office, Washington, DC, 1954.
21. R. Gray, *IEEE Trans. Info. Theory* **IT-18,** 725–730 (1972).